Structural and magnetic phase transitions of AV_6O_{11} (A = Na, Sr, and Pb)

2001 J. Phys.: Condens. Matter 13 9311

(http://iopscience.iop.org/0953-8984/13/41/319)

INSTITUTE OF PHYSICS PUBLISHING JOURNAL OF PHYSICS: CONDENSED MATTER

J. Phys.: Condens. Matter **13** (2001) 9311–9333 PII: S0953-8984(01)25086-3

Structural and magnetic phase transitions of AV_6O_{11} (A = Na, Sr, and Pb)

Harukazu Kato[1], **Masaki Kato, Kazuyoshi Yoshimura and Koji Kosuge**

Division of Chemistry, Graduate School of Science, Kyoto University, Sakyo-ku, Kyoto-fu 606-8502, Japan

E-mail: haru@kuchem.kyoto-u.ac.jp

Received 21 May 2001
Published 28 September 2001
Online at stacks.iop.org/JPhysCM/13/9311

Abstract

X-ray powder diffraction experiments have been made for mixed-valence vanadium compounds of AV_6O_{11} (A = Na, Sr, and Pb) between 12 and 700 K and their magnetic susceptibility has been measured between 5 and 700 K. It was revealed that each compound of AV_6O_{11} indicates a structural phase transition at $T_t = 245$ K for A = Na, 320 K for A = Sr and 560 K for A = Pb. This transition is accompanied by atomic displacement, leading to the formation of triangular trimers of the V(1) atoms, which construct a two-dimensional kagome lattice in AV_6O_{11}. The Curie constant C, the Weiss temperature Θ_p and the temperature-independent susceptibility χ_0 have been obtained in two temperature regions, $T < T_t$ and $T > T_t$. The abrupt reduction of C below T_t may indicate that the d-electrons of V(1) show a transition to a spin-singlet ground state at T_t.

1. Introduction

Mixed-valence vanadium compounds have been attracting much interest in solid-state chemistry and physics because novel magnetic and electric properties can be expected from the many oxidation states in various crystal structures. Recently, a V^{3+}–V^{4+} mixed-valence vanadium oxide of NaV_6O_{11} has been discovered by Roy *et al* [1]. Kanke *et al* [2] refined the crystal structure of NaV_6O_{11} at room temperature as shown in figure 1. This structure is hexagonal with the space group of $P6_3/mmc$. Hereafter, we call this structure the high temperature hexagonal (HTH) structure. In the HTH-structure, there exist three different kinds of vanadium sites: two octahedral sites, V(1) and V(2), and one trigonal-bipyramidal site, V(3). The V(1) octahedra share edges with each other and make a kagome lattice as shown in figure 2(a). Two V(2) octahedra form a face-sharing dimer along the c-axis. The V(3) site is located at $z = 1/4$ and $3/4$. The unit cell contains V(1), V(2) and V(3) with a ratio of 3:2:1. It has been reported that NaV_6O_{11} undergoes structural phase transitions at 245 and 80 K [3, 4]. The crystal structure between 245 and 80 K, which is defined as the low temperature

[1] Author to whom correspondence should be addressed.

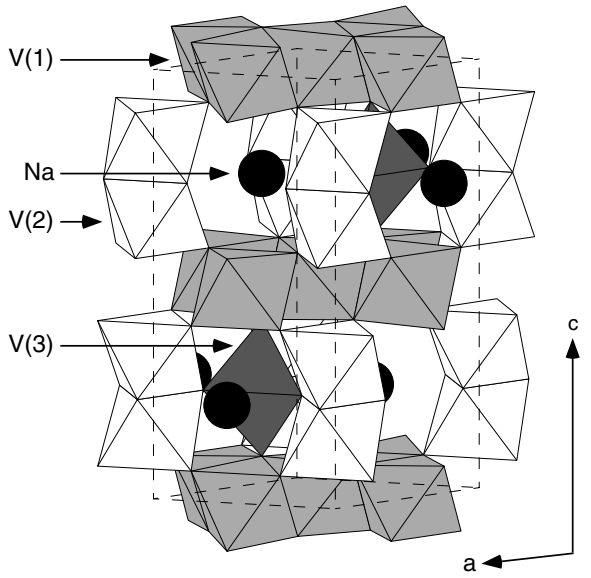

Figure 1. Crystal structure of NaV_6O_{11} at room temperature (HTH-structure). Dashed lines express a unit cell.

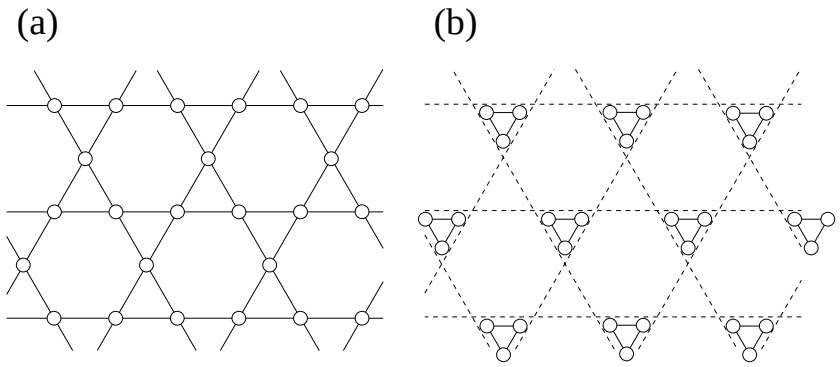

Figure 2. Kagome lattice of V(1) atoms. Open circles indicate V(1) atoms in (a) the HTH-structure and (b) LTH-structure.

hexagonal (LTH) structure, was determined with a neutron diffraction study [3]. Though the LTH-structure remains hexagonal, its space group symmetry is changed to $P6_3mc$. It should be noted that the V(1) kagome network in the LTH-structure is distorted and clustered into a V_3 trimer as shown in figure 2(b). As we discuss in this paper, the displacement of the V(1) atoms plays an important role in the magnetic properties of the compound. The V(2) sites split into two kinds of crystallographic sites, V(21) and V(22), in the LTH-structure since the V(3) atoms move slightly along the *c*-axis. The crystal structure below 80 K is called the orthorhombic(O) structure in this paper because it has an orthorhombic symmetry [3].

NaV_6O_{11} shows anomalies in magnetic susceptibility and electrical resistivity at 245 K [5, 6]. It is noted that these anomalies are accompanied by the structural transition from the HTH- to the LTH-structure. However, the origin of the transition has not been clarified. It has been reported that NaV_6O_{11} shows another magnetic transition at $T_C = 64.2$ K [5], below which spontaneous magnetization appears. With decreasing temperature from T_C, magnetization increases monotonically.

SrV_6O_{11} can be regarded as the compound obtained by the substitution of monovalent Na ion with divalent Sr ion in NaV_6O_{11} [7]. Previous structural studies have suggested that SrV_6O_{11} has the HTH-structure at room temperature [2] and exhibits no structural transition between 22 and 373 K [3]. However, it will be shown in this paper that these suggestions would be ambiguous or untrue. The magnetic susceptibility and electric resistivity of SrV_6O_{11} indicate anomalies at 320 K [8]. The magnetic behaviour of SrV_6O_{11} around 320 K is quite similar to that of NaV_6O_{11} around 245 K. The magnetization of SrV_6O_{11} is maximum at 70 K and shows some curious temperature dependence below 70 K [8].

A mixed valence vanadium compound of PbV_6O_{11} has been discovered in the Pb–V–O system [9]. The LTH-structure has been suggested for PbV_6O_{11} at room temperature [9]. Any structural studies except for [9] have not been made so far. The magnetic behaviour of PbV_6O_{11} below room temperature [9] seems to be quite similar to that of NaV_6O_{11} between 64 and 245 K and that of SrV_6O_{11} between 70 and 320 K. However, there has been no investigation of the magnetic properties of PbV_6O_{11} above room temperature. It has been reported that the magnetization of PbV_6O_{11} begins to increase around 100 K [9].

The present paper describes the results of x-ray diffraction (XRD) measurements carried out on AV_6O_{11} (A = Na, Sr, and Pb) at temperatures between 12 and 700 K. These results indicate that all the compounds undergo a similar phase transition at $T_t = 245$ K (A = Na), 320 K (A = Sr), and 560 K (A = Pb). It is indicated that all the compounds exhibit the HTH-structure above T_t and the LTH-structure below T_t. The magnetic properties between 5 and 700 K are also reported. From the quantitative analyses of magnetic susceptibility, we suggest that d-electrons at V(1) sites form a spin-singlet ground state below T_t. The formation of the nonmagnetic ground state seems to be in accord with the atomic displacement at T_t, resulting in the trimerization of the V(1) atoms.

2. Experimental details

The polycrystalline samples of NaV_6O_{11} were prepared from $NaVO_3$, V_2O_3 and V_2O_5 [6]. The stoichiometric mixtures of the starting compounds were pelletized and wrapped in a gold foil, and then sealed in an evacuated silica tube. The mixtures were heated in a furnace at 823 K for 12 h, and at 973 K for 7 days, then cooled slowly down to room temperature.

The polycrystalline samples of SrV_6O_{11} were prepared from $Sr_2V_2O_7$ and V_2O_3 [7]. The stoichiometric mixtures of the starting materials were pelletized and wrapped in a platinum foil, and then sealed in an evacuated silica tube. The mixtures were heated in a furnace at 1473 K for 1 day, cooled slowly down to 1273 K and then quenched to room temperature.

The polycrystalline samples of PbV_6O_{11} were prepared from PbO, V_2O_3 and V_2O_5. In order to compensate for the loss due to vaporization of Pb, the starting materials were mixed with 10% excess of Pb. The mixtures were pelletized and sealed directly into an evacuated silica tube without wrapping in any kind of foil. They were heated at 823 K for 12 h, then at 1213 K for 3 days and then quenched to room temperature to avoid formation of the impurity phase, $Pb_{1.32}V_{8.35}O_{16.7}$ [9].

The XRD data at various temperatures between 12 and 700 K were collected on MAC Science diffractometers with monochromatized Cu Kα radiation. For measurements below room temperature, the powder samples soaked in grease were pasted on a copper holder and were placed in an evacuated chamber having a beryllium window. For measurements above room temperature the samples were fixed on a platinum sample holder and settled in a sample space with N_2 gas flowing. The temperatures were controlled within ± 0.1 K. Scans were performed at 0.02° intervals.

Structural refinements were carried out at several temperatures. Since broad extra peaks appeared around $2\theta \sim 27^\circ$, we utilized the XRD data with $15^\circ < 2\theta < 27.5^\circ$ and $29^\circ < 2\theta < 80^\circ$ in the refinements. A Rietveld refinement program, RIETAN2000 [10], was used for the analyses of the XRD patterns. The isotropic thermal parameters for every atom were constrained to be equal.

Magnetic measurements were carried out between 5 and 700 K. For measurements below 350 K, we utilized a SQUID magnetometer (QUANTUM DESIGN, MPMS). The magnetization, M, on the zero field cooling (ZFC) and field cooling (FC) processes was measured under an applied field H of 1 T. At some temperatures, the magnetization curves were also measured up to an applied field of 5 T. M above 290 K was measured using a magnetic torsion balance under a magnetic field of 0.5715 T.

3. Results

3.1. NaV_6O_{11}

The XRD pattern at room temperature indicated that NaV_6O_{11} was almost composed in the HTH-phase with unit cell parameters $a = 5.694$ Å and $c = 13.059$ Å, though there exist traces of the impurity phases, α'–NaV_2O_5 and V_3O_5. The lattice parameters of the main phase are almost consistent with the previously reported values ($a = 5.7123$ Å and $c = 13.0974$ Å) [2].

The previous structural studies on NaV_6O_{11} [2, 3] have proposed that NaV_6O_{11} exhibits structural transitions at 245 and 80 K and have determined the structural parameters of the HTH-structure at room temperature, the LTH-structure at 200 K and the O-structure at 30 K. To confirm these suggestions, we have carried out XRD measurements for NaV_6O_{11} at several temperatures. Here, for ease in the following discussion for the structural transitions of SrV_6O_{11} and PbV_6O_{11}, we simulated the XRD patterns for each structure of NaV_6O_{11} using the reported parameters and compared them with our experimental results.

The results of the simulation are shown in figure 3 and table 1. First, we draw attention to the differences in the calculated profiles between the HTH- and LTH-structures. The calculated relative intensity of the 215 reflection in the LTH-structure is 1.42 times greater than in the HTH-structure. If NaV_6O_{11} indicates structural transition from the HTH- to the LTH-structure, it is expected that the 215 reflection increases in intensity below the transition temperature. The results of our XRD measurements for NaV_6O_{11} are shown in figure 4. We have observed enhancement of the intensity of the 215 reflection, $I_{215}(T)$, below 250 K. As shown in the inset of figure 4(a), $I_{215}(T)$ shows a clear temperature dependence and begins to increase around 250 K, while the intensities of the other reflections remain unchanged. Therefore, our results for NaV_6O_{11} give corroborative evidence for the structural transition from the HTH- to the LTH-structure at $T_t \sim 250$ K. We note that enhancement of the intensities of the 301, 303 and 207 reflections is expected from the simulated XRD patterns; however, the intensities of these reflections were so weak that we could not confirm the change of the intensities within the instrumental sensitivity.

Second, we discuss the transition from the LTH- to the O-structure. According to the simulated patterns, the structural transition to the O-structure should cause a change of the XRD profile, resulting in splits to the 302 and 214 reflection peaks as shown in the inset of figure 3. In fact, we have observed that the 302 and 214 reflection peaks split into multiple peaks below 80 K as shown in figure 4(b). Therefore, our results are consistent with the previous report that the structural transition to the O-structure takes place at 80 K [3, 4]. Consequently, our measurements confirm that NaV_6O_{11} shows structural transitions at 245 K (from the HTH- to the LTH-structure) and at 80 K (from the LTH- to the O-structure).

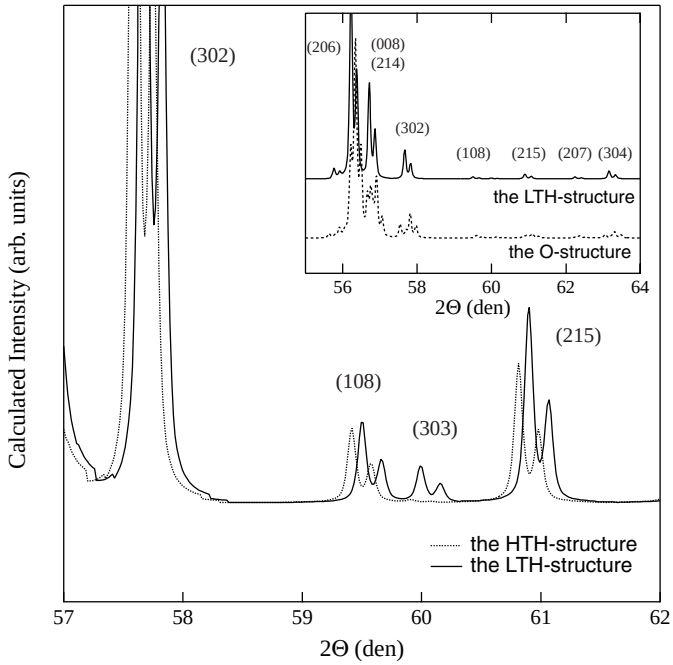

Figure 3. Calculated XRD patterns of NaV_6O_{11} for the HTH-structure, the LTH-structure and the O-structure.

Table 1. Calculated peak positions and intensities for the HTH- and the LTH-structures. The ratio of the intensities between the HTH- and LTH-structures is also shown.

			HTH-structure		LTH-structure		
H	K	L	$2\Theta_{cal}$ (deg)	I_{cal} (arb.units)	$2\Theta_{cal}$ (deg)	I_{cal} (arb.units)	Ratio
3	0	0	55.698	4 635	55.774	4 655	1.00
0	0	8	56.135	8 194	56.216	8 354	1.02
2	0	6	56.153	90 368	56.232	91 115	1.01
3	0	1	56.177	270	56.253	547	2.03
2	1	4	56.643	44 892	56.721	45 227	1.01
3	0	2	57.596	13 667	57.675	14 199	1.04
1	0	8	59.419	864	59.506	948	1.10
3	0	3	59.915	24	59.998	419	17.46
2	1	5	60.818	1 627	60.903	2 303	1.42
2	0	7	62.158	787	62.248	926	1.18
3	0	4	63.073	3 908	63.161	3 925	1.00

The temperature dependence of the magnetic susceptibility, χ ($=M/H$), is shown in figure 5(a). There appears an anomaly at $T_{t,mag} = 245$ K. It should be noted that $T_{t,mag}$ agrees well with T_t. The magnetic transition at $T_{t,mag}$ is accompanied by the structural transition at T_t. As shown in the inset of figure 5(a), χ^{-1} linearly depends on the temperature above $T_{t,mag}$, while the curvature of χ^{-1} below $T_{t,mag}$ is convex. These behaviours of χ^{-1} are the same as those reported previously [5, 6]. In section 4, we will give a probable explanation for the magnetic transition at $T_t = T_{t,mag}$.

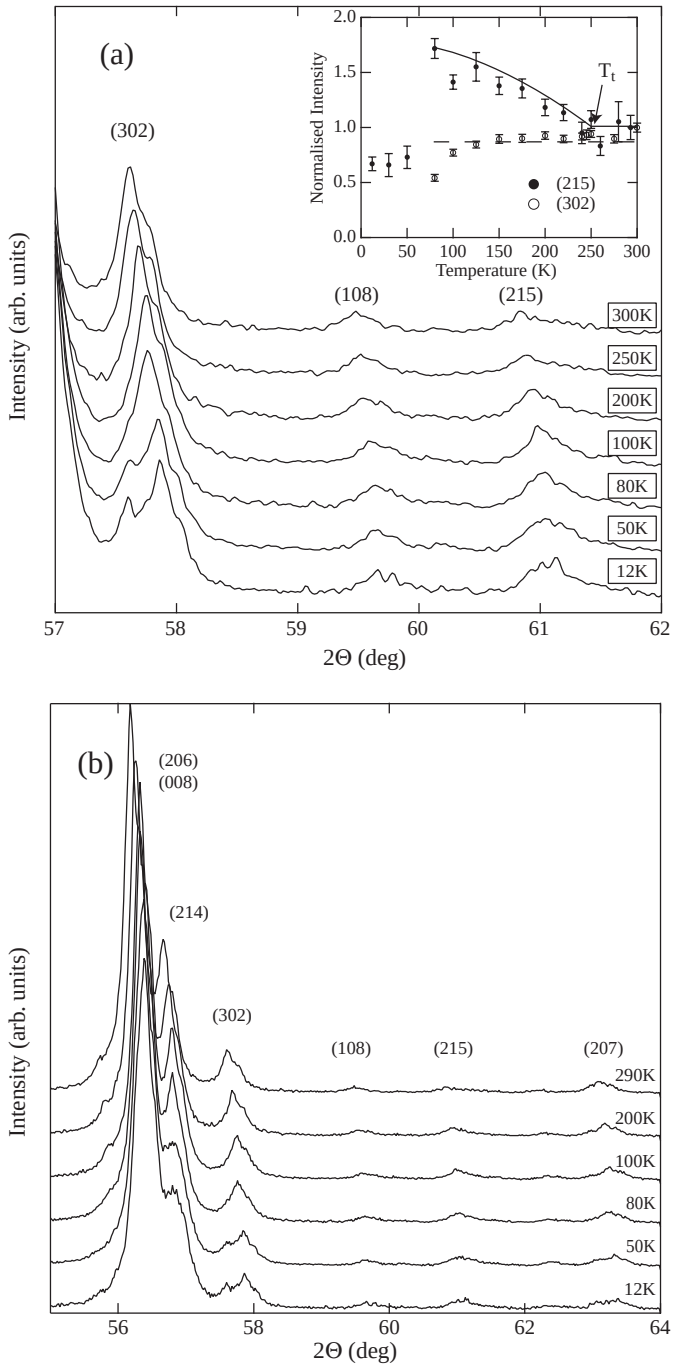

Figure 4. (a) Observed XRD patterns of NaV_6O_{11}. The inset indicates the temperature dependences of the intensities of the 215 (solid circles) and 302 (open circles) reflections. (b) Observed XRD patterns of NaV_6O_{11} with $55^\circ < 2\theta < 64^\circ$.

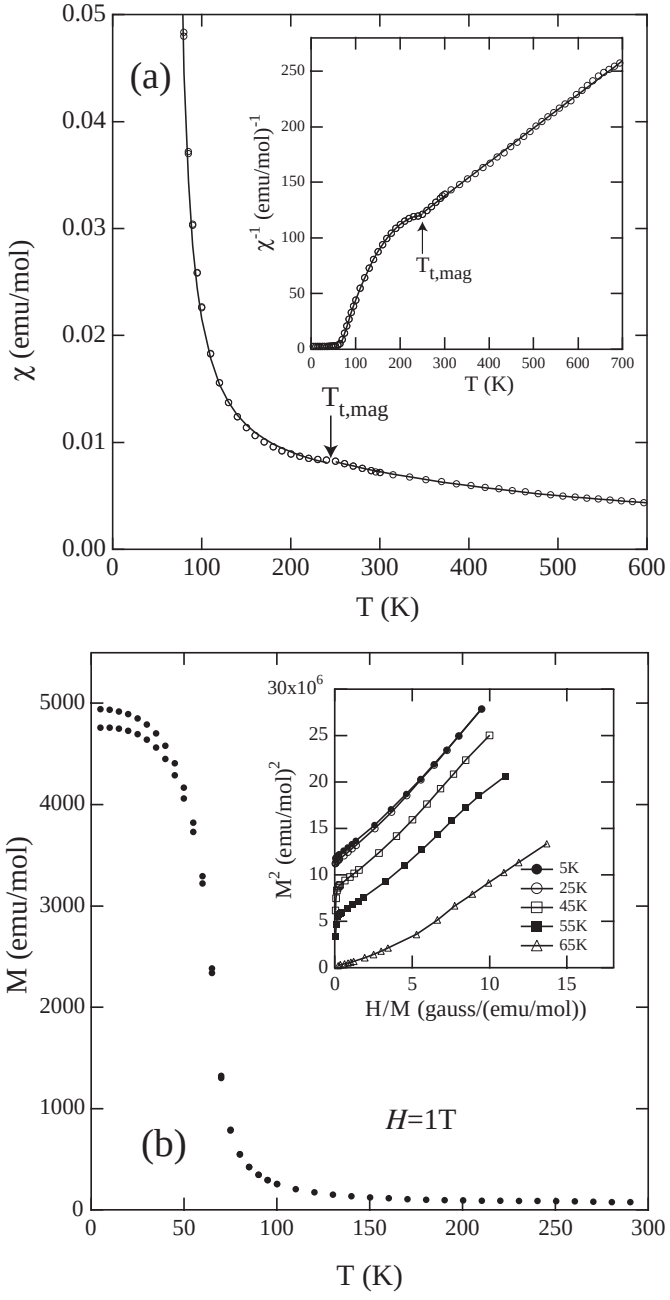

Figure 5. (a) Temperature dependence of χ of NaV_6O_{11}. The inset shows χ^{-1} plotted against temperature. (b) Temperature dependence of M of NaV_6O_{11} at $H = 1$ T. The inset shows the Arrott plot (see text).

Figure 5(b) shows the temperature dependence of M under $H = 1$ T. The magnetization rapidly increases and tends to saturate with decreasing temperature. These facts imply a ferromagnetic transition as reported previously [5, 6]. To determine the critical temperature,

we plot M^2 as a function of H/M, which is the so-called Arrott plot, in the inset of figure 5(b). Since the positive intercept on the vertical axis corresponds to the square of spontaneous magnetization, M_s^2, we can determine 65 K as the critical temperature T_C, where M_s becomes zero.

3.2. SrV_6O_{11}

From the XRD pattern at room temperature, SrV_6O_{11} was confirmed to be in a single phase with hexagonal unit cell dimensions of $a = 5.760$ Å and $c = 13.063$ Å. The lattice parameters are similar to the previously reported values ($a = 5.7716$ Å and $c = 13.0793$ Å) [2].

Previous structural studies [2, 3] have proposed that SrV_6O_{11} has the HTH-structure at room temperature [2] and indicate no structural transition between 22 and 350 K [3]. However, the following facts should be noted. First, the LTH-structure model gave a similar R value to the HTH-structure model at room temperature [2]. This does not disallow the LTH-structure as the structure of SrV_6O_{11} at room temperature. Second, it has been reported that SrV_6O_{11} shows an anomaly at 320 K in magnetic susceptibility [8] and that its magnetic behaviour around 320 K is quite similar to that of NaV_6O_{11} around 245 K [8]. Since the magnetic transition in NaV_6O_{11} at 245 K is accompanied by a structural transition as confirmed above, it may be expected that SrV_6O_{11} also shows the structural transition from the HTH- to the LTH-structure at 320 K.

Considering these points at issue, we carried out XRD measurements at various temperatures for SrV_6O_{11}. The results are shown in figure 6(a) and (b). As indicated in figure 6(a), the intensity of the 215 reflection increases with decreasing temperature. The inset of figure 6(a) shows $I_{215}(T)$ plotted against temperature. Here, the obtained data were normalized by the value at room temperature. It is shown that $I_{215}(T)$ begins to increase around 300 K, while the intensities of the other reflections are found to be almost independent of temperature. This gives clear evidence that SrV_6O_{11} shows a structural phase transition at $T_t \sim 300$ K. Furthermore, it is to be noted that NaV_6O_{11}, which exhibits the structural transition from the HTH- to the LTH-structure at 245 K, indicates an enhancement of the intensity of the 215 reflection (see figures 3 and 4(a)). It is natural to assume that SrV_6O_{11} shows the structural transition at T_t from the HTH- to the LTH-structure.

To clarify the structural transition, we have refined the structural parameters of SrV_6O_{11} at two temperatures of 623 K ($\gg T_t$) and 100 K ($\ll T_t$). First, we mention the results of the refinements for 623 K ($\gg T_t$). The refinement using the HTH-structure model gave a unit cell of $a = 5.8067$ Å and $c = 13.1900$ Å and converged to $R_{WP} = 9.91\%$, $R_P = 7.57\%$ and $R_e = 4.48\%$. Since the value of R_{WP} is less than 10% and the latter two R values are so small, our structural refinement of SrV_6O_{11} is reliable. The observed and calculated XRD patterns are shown in figure 7(a). The refined structural parameters at 623 K are shown in table 2(a). Since the HTH-structure has the space group of $P6_3/mmc$, the V(1) atoms at the 6*g* position (1/2, 1/2, 0) form a kagome lattice as shown in figure 2(a). Selected interatomic distances are presented in table 3(a). Second, we discuss the structure at 100 K ($\ll T_t$). The refinement using the LTH-structure model gave a unit cell of $a = 5.7569$ Å and $c = 13.0805$ Å and converged to $R_{WP} = 9.64\%$, $R_P = 6.64\%$, and $R_e = 4.03\%$. The small R values indicate that our refinement at 100 K is successful. Figure 7(b) shows the observed and calculated XRD patterns at 100 K. The refined structural parameters at 100 K are shown in table 2(b). It should be noted that the V(1) atoms are displaced from the position (1/2, 1/2, 0) beyond experimental uncertainty. This indicates that the kagome lattice formed in the HTH-structure is distorted in the LTH-structure. Since the V(1) atoms are located at the 6*c* position with the space group of $P6_3mc$, the triangular clusters of the V(1) atoms as shown in figure 2(b) are formed in the

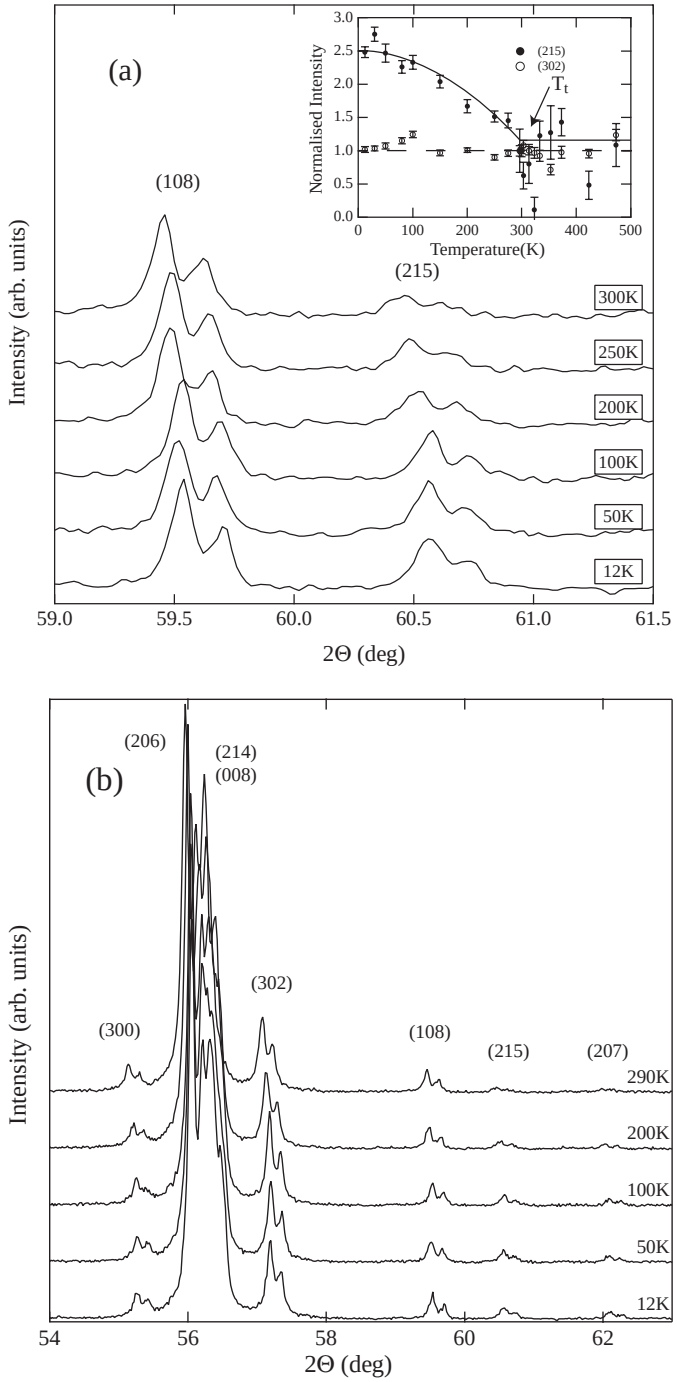

Figure 6. (a) Observed XRD patterns of SrV_6O_{11}. The inset indicates temperature dependences of the intensities of the 215 (solid circles) and 302 (open circles) reflections. (b) Observed XRD patterns of SrV_6O_{11} with $55^\circ < 2\theta < 64^\circ$.

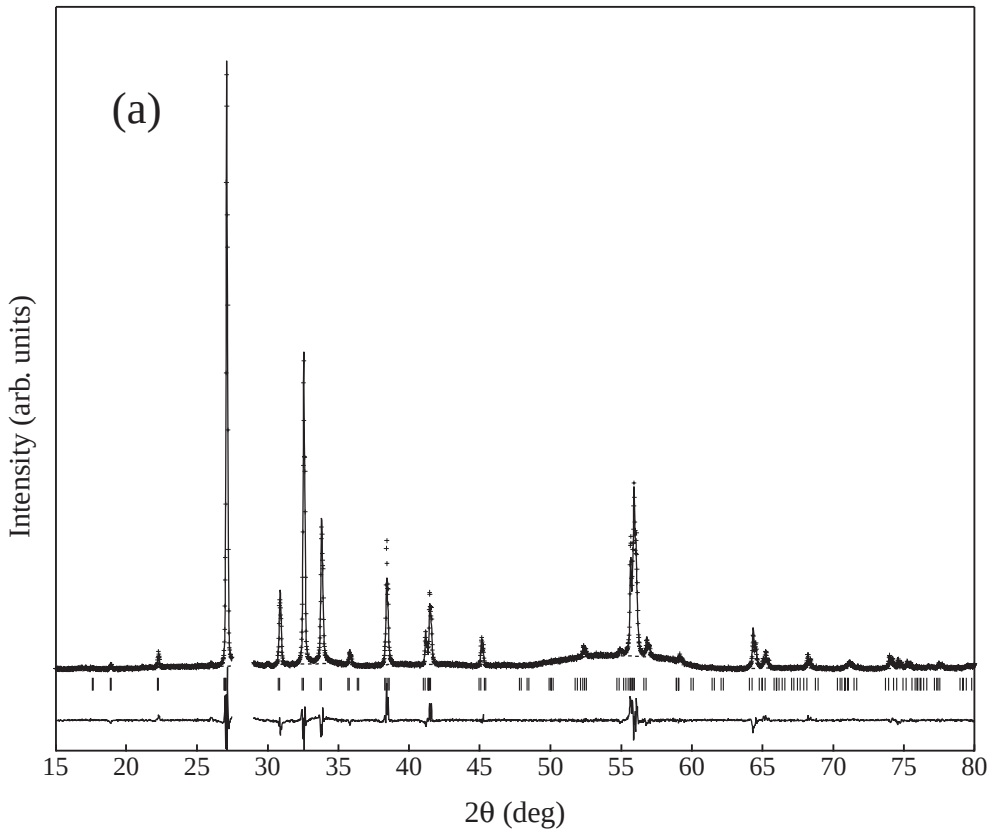

Figure 7. Observed (crosses) and calculated (solid line) XRD profiles of SrV_6O_{11} at 623 K (a) and 100 K (b). Broken lines represent the background intensities. Short vertical bars indicate the positions of allowed Bragg reflection. The differences between observed and calculated values are located at the bottom of each of the figures.

LTH-structure. Selected interatomic distances are presented in table 3(b). The V(1)–V(1) distance in the LTH-structure falls into two categories, corresponding to the formation of the trimers. Several attempts were made to refine by using the HTH-structure model; however, they gave rather higher R values ($R_{WP} \sim 14\%$, $R_P \sim 9.4\%$, and $R_e \sim 4\%$) and even negative thermal parameters for some atom positions. Therefore, we conclude that SrV_6O_{11} has the HTH-structure at 623 K and the LTH-structure at 100 K. Consequently, from the results of the refinements at two temperatures, we conclude that SrV_6O_{11} indicates a structural transition from the HTH- to the LTH-structure at T_t.

As mentioned above, NaV_6O_{11} indicates a transition to the O-structure at 80 K, which causes peak splits in the XRD profile. In contrast to the case in NaV_6O_{11}, we could not find any splits in the reflection peaks in the profiles of SrV_6O_{11} at every temperature between 12 and 700 K as shown in figure 6(b). This indicates that SrV_6O_{11} does not show a transition from the LTH- to the O-structure at least down to 12 K. That is, while NaV_6O_{11} has two structural transition temperatures of 245 K ($=T_t$) and 80 K, SrV_6O_{11} shows a structural transition at only one temperature of $T_t \sim 300$ K and maintains the LTH-structure even at low temperature.

Figure 8(a) shows the temperature dependence of χ of SrV_6O_{11}. SrV_6O_{11} has a magnetic anomaly at $T_{t,mag} = 320$ K. Agreement between $T_{t,mag}$ and T_t indicates that structural and

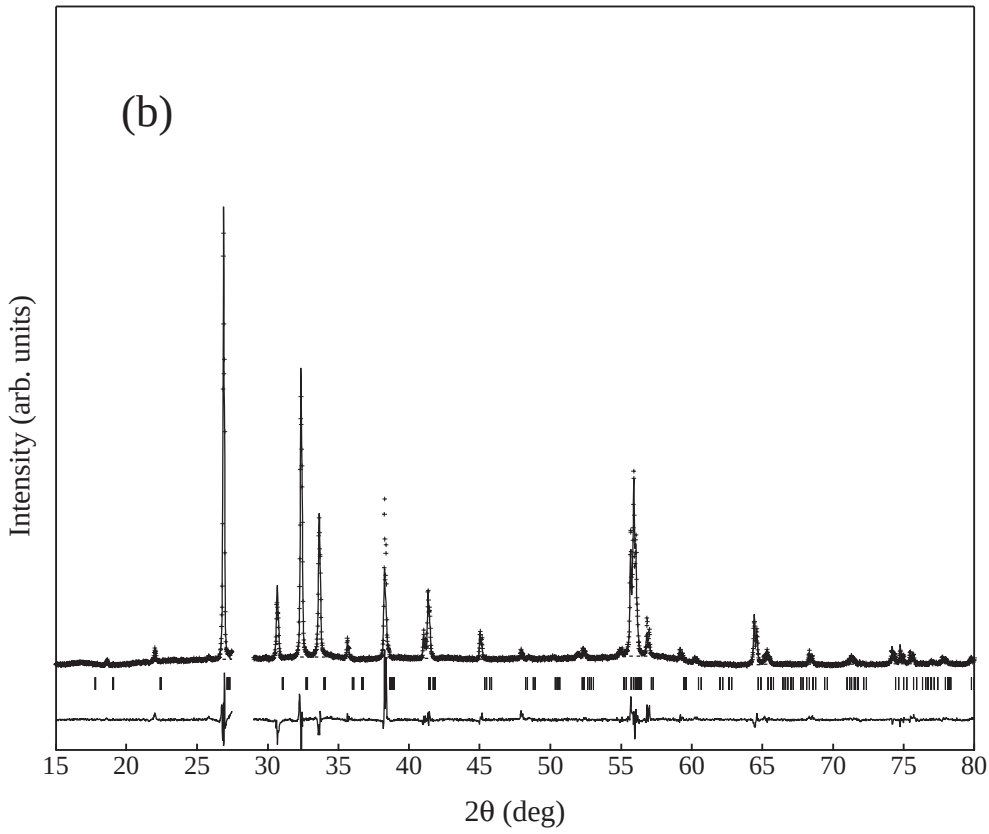

Figure 7. (*Continued*)

magnetic transitions occur simultaneously. The curvature of χ^{-1} above $T_{t,mag}$ is linear, while below $T_{t,mag}$ it is convex. These behaviours of χ^{-1} are similar to those in NaV_6O_{11}. It is expected that the magnetic transition at $T_{t,mag}$ in SrV_6O_{11} are identical to those in NaV_6O_{11}, although the average vanadium valence differs between the Sr-compound and the Na-compound.

In figure 8(b), we show the temperature dependence of M at $H = 1$ T. The Arrott plot in the inset of figure 8(b) indicates that spontaneous magnetization appears below $T_C = 75$ K. With decreasing temperature from T_C, M increases rapidly and shows a maximum at 50 K. The temperature where M has the maximal value is slightly different from 70 K, which has been reported previously [8]. The reason for the discrepancy is not clear. Nevertheless, it is certain that magnetic behaviour below T_C of SrV_6O_{11} is quite different from that of NaV_6O_{11}.

3.3. PbV_6O_{11}

From the XRD pattern at room temperature, PbV_6O_{11} was confirmed to be in a single phase with hexagonal unit cell dimensions of $a = 5.756$ Å and $c = 13.270$ Å. These values are in good agreement with previously reported values ($a = 5.754$ Å and $c = 13.267$ Å) [9].

Figure 9(a) shows the XRD patterns of PbV_6O_{11} at various temperatures. The inset of figure 9(a) shows the temperature dependence of $I_{215}(T)$. One can easily find that $I_{215}(T)$

Table 2. Positional parameters and equivalent thermal parameters in SrV_6O_{11} at (a) 623 K and (b) 100 K.

Atom	Site	x	y	z	B_{eq} (Å^2)
		(a) 623 K			
Sr	2c	1/3	2/3	1/4	2.5(2)
V(1)	6g	1/2	1/2	0	1.2(1)
V(2)	4e	0	0	0.145(1)	1.2(1)
V(3)	2d	2/3	1/3	1/4	1.2(1)
O(1)	12k	0.168(1)	−0.168(1)	0.084(1)	1.6(1)
O(2)	6h	0.151(2)	−0.151(2)	3/4	1.6(1)
O(3)	4f	2/3	1/3	0.416(1)	1.6(1)
		(b) 100 K			
Sr	2b	1/3	2/3	0.254(2)	2.6(2)
V(1)	6c	0.505(1)	−0.505(1)	0.005(3)	0.6(1)
V(21)	2a	0	0	0.149(3)	0.6(1)
V(22)	2a	0	0	0.358(3)	0.6(1)
V(3)	2a	2/3	1/3	0.268(3)	0.6(1)
O(11)	6c	0.179(2)	−0.179(2)	0.084(3)	0.1(2)
O(12)	6c	0.153(2)	−0.153(2)	0.429(4)	0.1(2)
O(2)	6c	0.162(3)	−0.162(3)	0.764(3)	0.1(2)
O(31)	2b	2/3	1/3	0.100(3)	0.1(2)
O(32)	2b	2/3	1/3	0.405(4)	0.1(2)

Table 3. Selected interatomic distances (Å) of SrV_6O_{11} at (a) 623 K and (b) 100 K.

(a) 623 K		(b) 100 K	
Bond	Distance	Bond	Distance
V(1)–O(1)	2.00(1)	V(1)–O(11)	1.94(1)
		V(1)–O(12)	1.98(2)
V(1)–O(3)	2.00(1)	V(1)–O(31)	2.03(1)
		V(1)–O(32)	2.16(1)
V(2)–O(1)	1.87(2)	V(21)–O(11)	1.98(3)
		V(22)–O(12)	1.78(2)
V(2)–O(2)	2.06(2)	V(21)–O(2)	2.20(3)
		V(22)–O(2)	2.04(2)
V(3)–O(2)	1.83(2)	V(3)–O(2)	1.71(2)
V(3)–O(3)	2.19(1)	V(3)–O(31)	2.19(2)
		V(3)–O(32)	1.80(2)
Sr–O(1)	2.75(1)	Sr–O(11)	2.70(2)
		Sr–O(12)	2.7(3)
Sr–O(2)	2.91(1)	Sr–O(2)	2.91(1)
V(1)–V(1)	2.90(1)	V(1)–V(1) (intra-trimer)	2.79(2)
		V(1)–V(1) (inter-trimer)	2.97(2)
V(2)–V(2)	2.78(3)	V(21)–V(22)	2.74(1)
V(3)–V(3)	5.81(1)	V(3)–V(3)	5.76(1)

begins to increase at about 600 K while the other reflections are independent of temperature. It is clear that PbV_6O_{11} shows a structural transition at $T_t \sim 600$ K.

Taking account of the case with NaV_6O_{11} and SrV_6O_{11}, we suppose that PbV_6O_{11} also shows a structural transition from the HTH- to the LTH-structure because the intensity of the

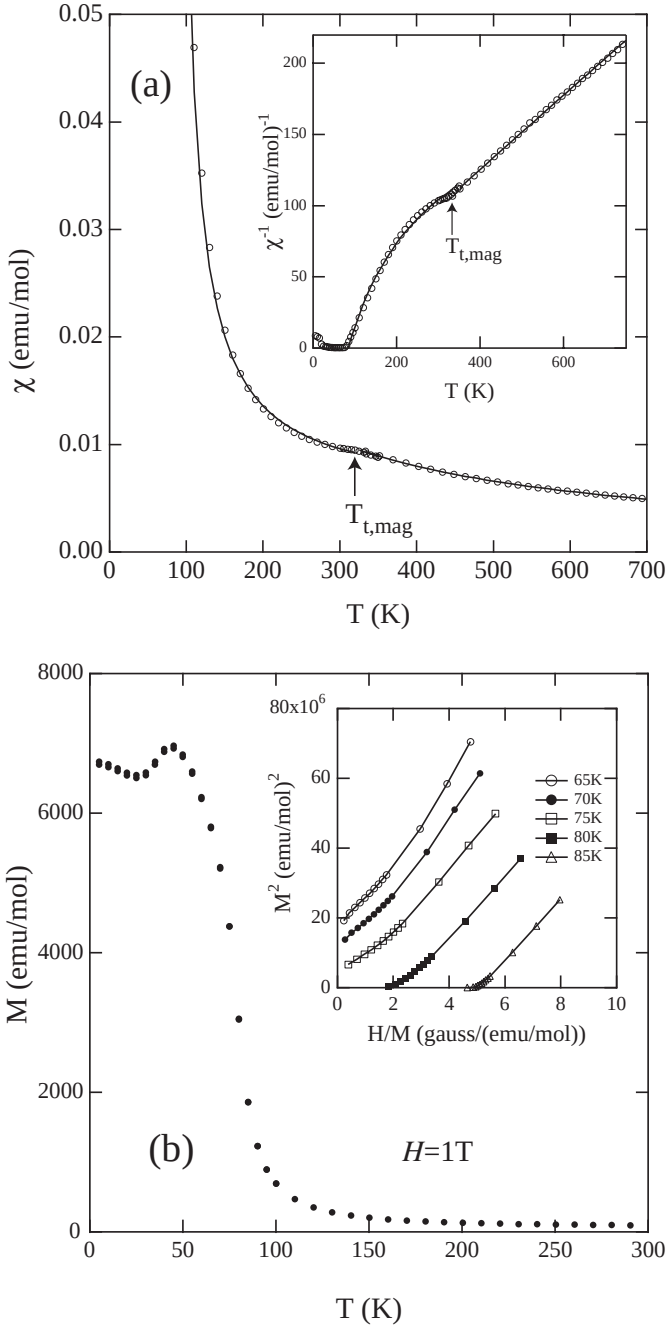

Figure 8. (a) Temperature dependence of χ of SrV_6O_{11}. The inset shows χ^{-1} plotted against temperature. (b) Temperature dependence of M of SrV_6O_{11} at $H = 1$ T. The inset shows the Arrott plot (see text).

215 reflection is clearly dependent on temperature. To confirm this suggestion, we have tried to determine the structures of PbV_6O_{11} at 623 K ($>T_t$) and 100 K ($\ll T_t$). First, we mention the result of the refinement at 623 K ($>T_t$). The refinement using the HTH-structure model

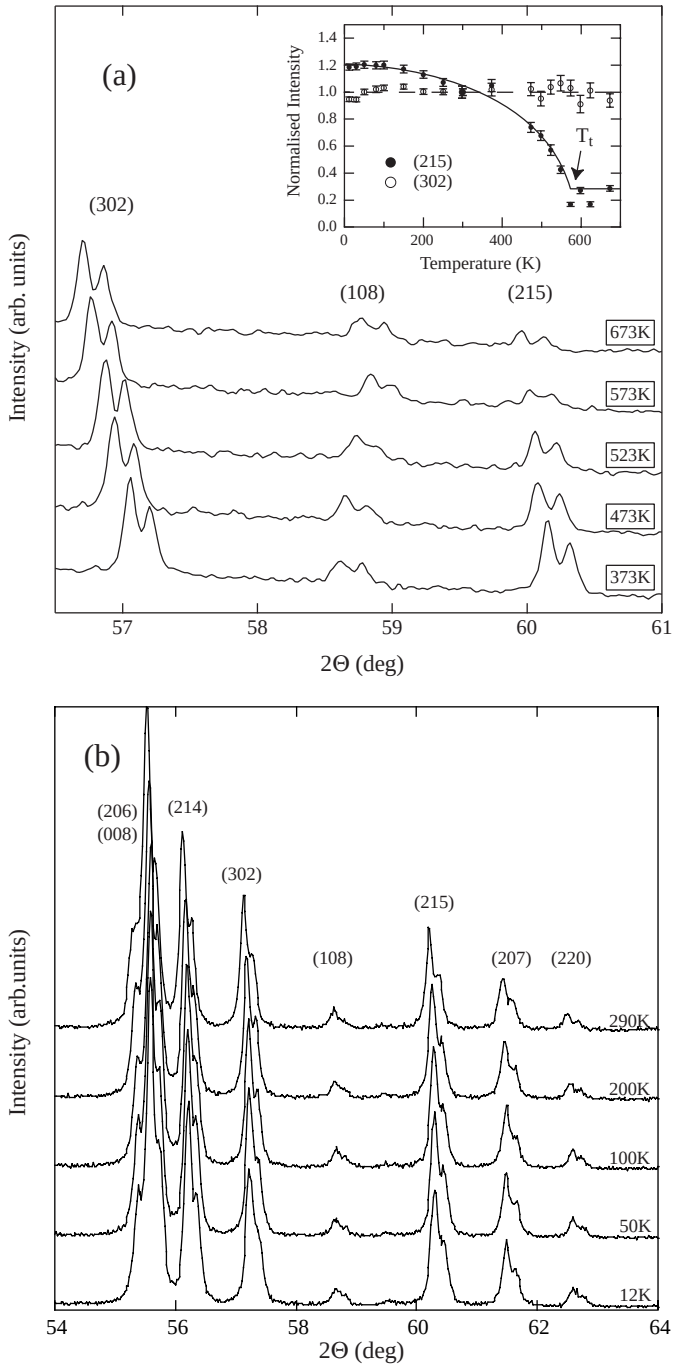

Figure 9. (a) Observed XRD patterns of PbV_6O_{11}. The inset indicates temperature dependences of the intensities of the 215 (solid circles) and 302 (open circles) reflection. (b) Observed XRD patterns of PbV_6O_{11} with $55^\circ < 2\theta < 64^\circ$.

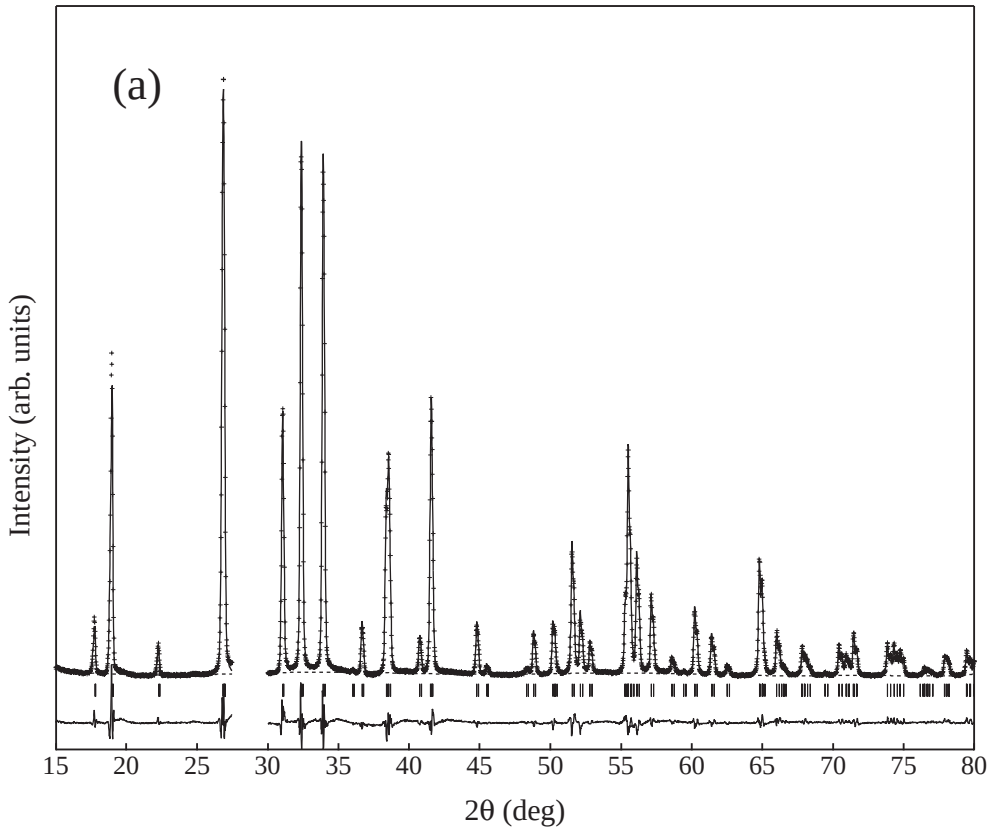

Figure 10. Observed (crosses) and calculated (solid line) XRD profiles of PbV_6O_{11} at (a) 623 K and (b)100 K. Broken lines represent background intensities. Short vertical bars indicate the positions of allowed Bragg reflection. The differences between observed and calculated values are located at the bottom of each of the figures.

gave a unit cell of $a = 5.8310$ Å and $c = 13.3008$ Å, and converged to $R_{WP} = 8.69\%$, $R_P = 6.69\%$ and $R_e = 4.04\%$. Since the value of R_{WP} is less than 10% and the latter two R values are so small, our structural refinement of SrV_6O_{11} is reliable. The results of the refinement at 623 K are shown in figure 10(a) and table 4(a). Since the HTH-structure has the space group of $P6_3/mmc$, the V(1) atoms at the 6g position (1/2, 1/2, 0) form a kagome lattice as shown in figure 2(a). Selected interatomic distances are presented in table 5(a). Second, we discuss the structure at 100 K ($\ll T_t$). The refinement using the LTH-structure model gave a unit cell of $a = 5.7508$ Å and $c = 13.2701$ Å and converged to $R_{WP} = 8.59\%$, $R_P = 6.36\%$ and $R_e = 3.22\%$. The small R values indicate that our refinement at 100 K is successful. Figure 10(b) shows the observed and calculated XRD patterns at 100 K. The refined structural parameters at 100 K are shown in table 4(b). As is the case with SrV_6O_{11}, the V(1) atoms are displaced from the position (1/2, 1/2, 0) beyond experimental uncertainty, indicating the distortion of the kagome lattice. Selected interatomic distances are presented in table 5(b). Note that the V(1)–V(1) distance in the LTH-structure falls into two categories corresponding to the formation of the trimers as shown in figure 2(b). Several attempts at refinement were made using the HTH-structure model; however, they gave rather higher R values

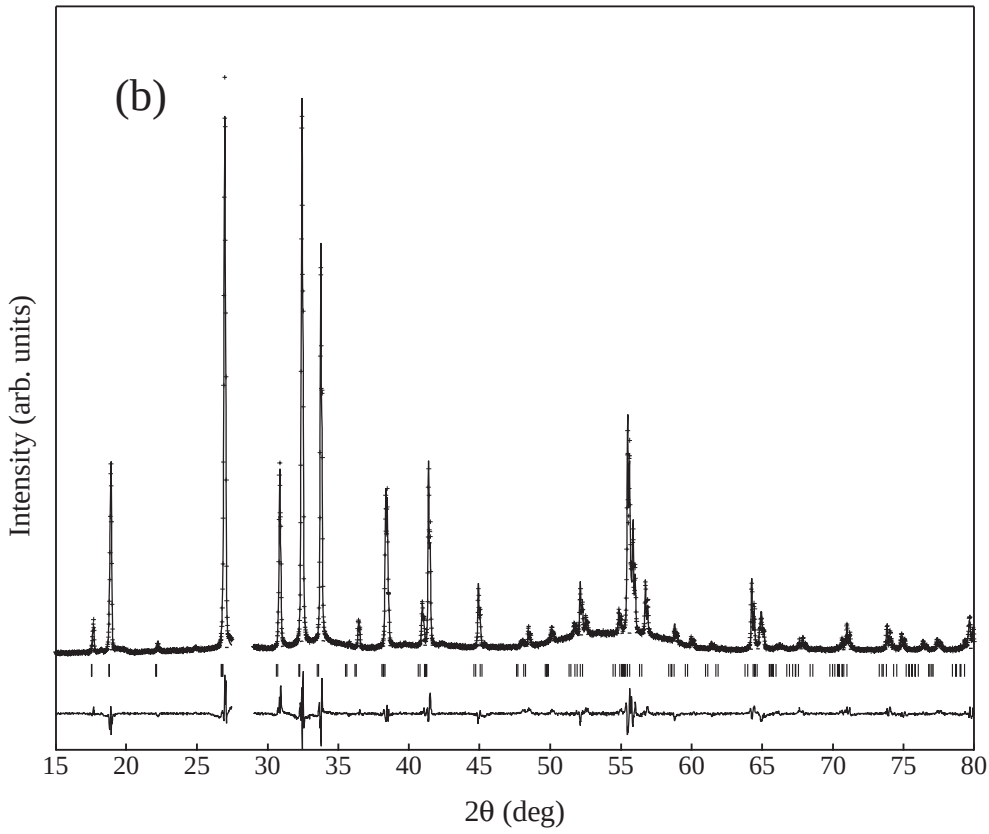

Figure 10. (*Continued*)

($R_{WP} \sim 16\%$, $R_P \sim 12\%$ and $R_e \sim 3\%$) and even negative thermal parameters for some atomic positions. Therefore, we conclude that PbV_6O_{11} has the HTH-structure at 623 K and the LTH-structure at 100 K. Consequently, we found that PbV_6O_{11} also indicates the structural transition at T_t from the HTH- to the LTH-structure. Our argument is consistent with the previous structural study [9] suggesting the LTH-structure at room temperature.

As is shown in figure 9(b), we could not obtain any evidence of another structural transition such as a transition to the O-structure in NaV_6O_{11}. As is the case with SrV_6O_{11}, it seems that PbV_6O_{11} shows a structural transition at only one temperature of T_t and maintains the LTH-structure even at the lowest temperature.

In figure 11(a), we show the temperature dependence of χ of PbV_6O_{11} between 5 and 700 K. There exists an anomaly in χ at $T_{t,mag} = 560$ K, which agrees well with $T_t \sim 600$ K. It is found that the magnetic transition of PbV_6O_{11} at $T_{t,mag}$ is accompanied by a structural transition. As is the case with the other two compounds, the curvature of χ^{-1} above $T_{t,mag}$ is linear to T while that below $T_{t,mag}$ is convex.

Figure 11(b) shows the temperature dependence of M at $H = 1$ T. The magnetization rapidly increases around 100 K. From the Arrott plot in the inset of figure 11(b), T_C is estimated to be 85 K. A small drop in magnetization is observed at about 55 K and a broad maximum appears around 20 K. These behaviours of magnetization below T_C are in agreement with those reported previously [9].

Table 4. Positional parameters and equivalent thermal parameters in PbV_6O_{11} at (a) 623 K and (b) 100 K.

Atom	Site	x	y	z	B_{eq} (Å^2)
			(a) 623 K		
Pb	2c	1/3	2/3	1/4	4.1(1)
V(1)	6g	1/2	1/2	0	1.1(1)
V(2)	4e	0	0	0.147(1)	1.1(1)
V(3)	2d	2/3	1/3	1/4	1.1(1)
O(1)	12k	0.167(1)	−0.167(1)	0.075(1)	0.6(1)
O(2)	6h	0.151(1)	−0.151(1)	3/4	0.6(1)
O(3)	4f	2/3	1/3	0.410(1)	0.6(1)
			(b) 100 K		
Pb	2b	1/3	2/3	0.216(1)	0.9(1)
V(1)	6c	0.513(1)	−0.513(1)	−0.004(1)	0.6(1)
V(21)	2a	0	0	0.147(1)	0.6(1)
V(22)	2a	0	0	0.349(1)	0.6(1)
V(3)	2a	2/3	1/3	0.261(1)	0.6(1)
O(11)	6c	0.177(1)	−0.177(1)	0.075(1)	0.6(1)
O(12)	6c	0.151(1)	−0.151(1)	0.417(1)	0.6(1)
O(2)	6c	0.172(1)	−0.172(1)	0.747(1)	0.6(1)
O(31)	2b	2/3	1/3	0.086(2)	0.6(1)
O(32)	2b	2/3	1/3	0.417(2)	0.6(1)

Table 5. Selected interatomic distances (Å) of PbV_6O_{11} at (a) 623 K and (b) 100 K.

(a) 623 K		(b) 100 K	
Bond	Distance	Bond	Distance
V(1)–O(1)	1.95(1)	V(1)–O(11)	1.98(1)
		V(1)–O(12)	1.99(1)
V(1)–O(3)	2.07(1)	V(1)–O(31)	1.94(1)
		V(1)–O(32)	2.07(1)
V(2)–O(1)	1.94(1)	V(21)–O(11)	2.00(1)
		V(22)–O(12)	1.75(1)
V(2)–O(2)	2.05(1)	V(21)–O(2)	2.16(1)
		V(22)–O(2)	2.18(1)
V(3)–O(2)	1.84(1)	V(3)–O(2)	1.62(2)
V(3)–O(3)	2.12(2)	V(3)–O(31)	2.32(2)
		V(3)–O(32)	2.08(2)
Pb–O(1)	2.87(1)	Pb–O(11)	2.44(1)
		Pb–O(12)	3.22(1)
Pb–O(2)	2.92(1)	Pb–O(2)	2.90(1)
V(1)–V(1)	2.92(1)	V(1)–V(1)(intra-trimer)	2.65(1)
		V(1)–V(1) (inter-trimer)	3.09(1)
V(2)–V(2)	2.75(1)	V(21)–V(22)	2.68(1)
V(3)–V(3)	5.83(1)	V(3)–V(3)	5.75(1)

4. Discussion

Our XRD measurements have revealed that not only NaV_6O_{11} but also SrV_6O_{11} and PbV_6O_{11} show a structural phase transition from the HTH- to the LTH-structure at $T_t = T_{t,mag} = 245$ K

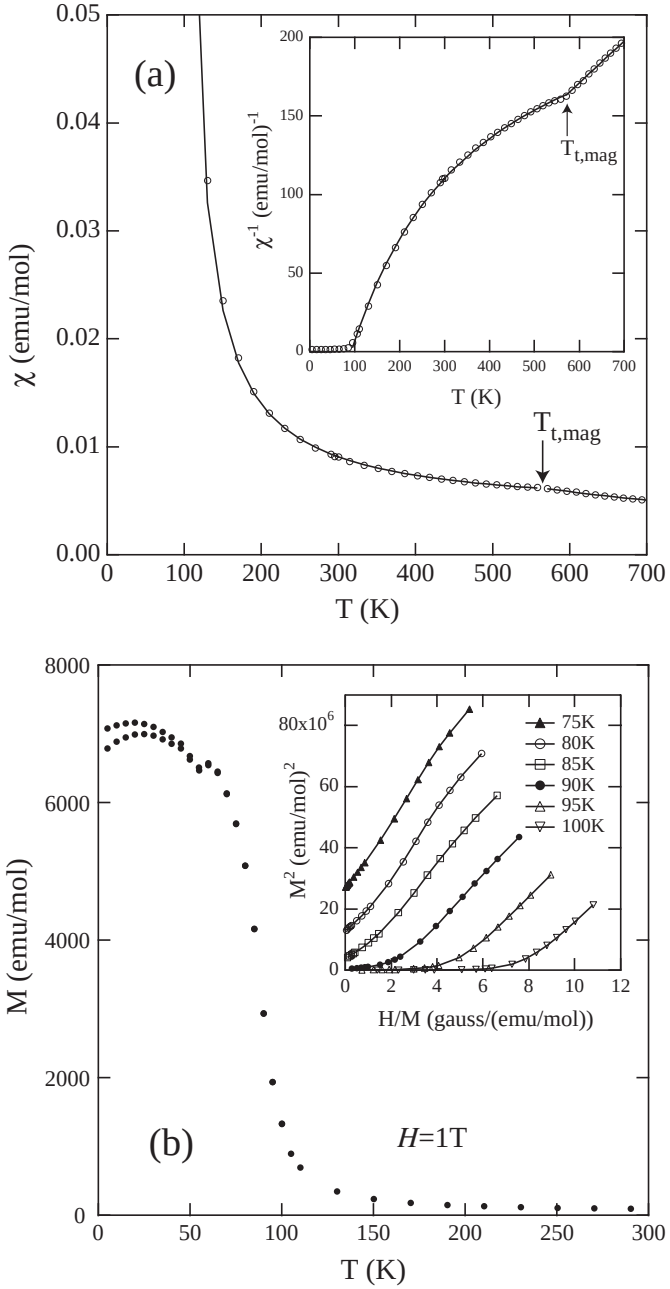

Figure 11. (a) Temperature dependence of χ of PbV_6O_{11}. The inset shows χ^{-1} plotted against temperature. (b) Temperature dependence of M of PbV_6O_{11} at $H = 1$ T. The inset shows the Arrott plot (see text).

(A = Na), 320 K (A = Sr), and 560 K (A = Pb). With regard to the latter two compounds, we give the first evidence on structural transitions. The structural transition at T_t of AV_6O_{11} is marked by the displacement of the V(1) atoms, which causes distortion of the kagome lattice and formation of the triangular clusters of the V(1) atoms in the LTH-structure below T_t. From

the viewpoint of magnetism, we will discuss the atomic displacement accompanied with the transition at T_t later.

Our magnetic measurements have clearly shown that AV_6O_{11} has an anomaly at $T_t = T_{t,mag}$ in magnetic susceptibility. It is noteworthy that the anomalies at T_t in these compounds are similar to one another, while the average valence of the vanadium atoms of NaV_6O_{11} (A^+ member) are different from those of SrV_6O_{11} and PbV_6O_{11} (A^{2+} members). According to the Curie–Weiss law including the temperature-independent susceptibility χ_0, the magnetic susceptibility is expressed by

$$\chi = \frac{C}{T - \Theta_p} + \chi_0 \tag{1}$$

where C denotes a Curie constant and Θ_p a Weiss temperature. The observed susceptibilities were fitted by equation (1) in the two temperature regions, $T_C < T < T_t$ and $T_t < T$. The solid lines in figures 5(a), 8(a), and 11(a) are the best results of the least-square fitting. The obtained values of C, Θ_p and χ_0 are shown in table 6. These parameters in the lower temperature region are quite different from those in the higher temperature region as follows: (1) the Curie constants in the lower temperature region, $C(T_C < T < T_t)$, are fairly smaller than those in the higher temperature region, $C(T_t < T)$, (2) the Weiss temperature in the lower temperature region is positive while in the higher temperature region it is negative, and (3) the value of χ_0 in the lower temperature region is relatively large while in the higher temperature region it is relatively small. Especially, the large value of χ_0 below T_t corresponds to the divergence from the linear temperature dependence of χ^{-1}.

Table 6. Curie constants, Weiss temperature and temperature-independent susceptibilities in (a) low ($T_C < T < T_t$) and (b) high temperature region ($T_t < T$).

	C (emu/mol K)	Θ_p (K)	$\chi_0 \times 10^3$ (emu/mol)
	(a) $T_C < T < T_t$		
NaV_6O_{11}	0.58(9)	65.3(6)	4.8(6)
SrV_6O_{11}	1.00(12)	84.8(11)	5.0(6)
PbV_6O_{11}	1.08(3)	92.6(4)	3.9(1)
	(b) $T_t < T$		
NaV_6O_{11}	3.1(2)	−140(11)	−0.1(1)
SrV_6O_{11}	3.6(2)	−63(8)	−0.2(1)
PbV_6O_{11}	3.7(1)	−32(5)	0.9(1)

Table 7. (a) Numbers in a unit cell of AV_6O_{11} and valences of the three vanadium sites, V(1), V(2) and V(3). The calculated values of the Curie constants C_i (expressed in units of mol of FU) are also shown for $i = 1$, 2, and 3 (see text). (b) Possible combinations of C_i.

(a)		Number of site	Valence	C_i (emu/mol K)
V(1)		3	+3	3.00
V(2)		2	+4	0.75
V(3)	A = Na	1	+4	0.38
	A = Sr, Pb		+3	1.00

(b)	$C_1 + C_2$	$C_1 + C_3$	$C_2 + C_3$	$C_1 + C_2 + C_3$
A = Na	3.75	3.38	1.13	4.13
A = Sr, Pb	3.75	4.00	1.75	4.75

According to the valence bond calculation [2], the valence of vanadium ions is estimated as shown in table 7(a). Because V^{3+} has two d-electrons and V^{4+} has one d-electron, it is expected that V(1) and V(2) have $S = 1$ and $1/2$, respectively, and V(3) in NaV_6O_{11} has $S = 1/2$ and V(3) in the other two compounds has $S = 1$, if these d-electrons are localized. Now, we calculate C_i ($i = 1$, 2 and 3), the Curie constants per one mole of AV_6O_{11} which are produced by the paramagnetic spin at the V(i) site. In general, the Curie constant C is written as

$$C = \frac{N\mu_{\text{eff}}^2}{3k_{\text{B}}} \qquad \mu_{\text{eff}} = g\sqrt{S(S+1)} \tag{2}$$

for an ionic system. Here, N is the number of the magnetic atoms, k_{B} the Boltzmann constant, and g the g-factor. S denotes the total quantum spin number of a magnetic ion; μ_{eff} is called the effective moment. If each vanadium site has paramagnetic moments accompanied with spins as mentioned above, we can estimate the value of C_i ($i = 1$, 2, 3) from equation (2). The results and their combination are shown in tables 7(a) and (b).

When all the d-electrons are magnetic and the corresponding paramagnetic moments exist at each vanadium site, the Curie constant of AV_6O_{11} should be equal to $C_1 + C_2 + C_3$ (=4.13 emu/mol K (A = Na), 4.75 emu/mol K (A = Sr) and 4.75 emu/mol K (A = Pb)). However, one can find that the observed values of $C(T_{\text{t}} < T)$ are smaller than the values of $C_1 + C_2 + C_3$. This may imply that a part of the d-electrons falls in a nonmagnetic state even above T_{t}. In fact, the presence of nonmagnetic vanadium ions above and below T_{t} is indicated by the previous ^{51}V-NMR study of NaV_6O_{11} [8] carried out from about 100 to 300 K. As mentioned above, the V(2) octahedra share a face in the dimer-like arrangement in the HTH-, LTH- and O-structures. It is quite natural that the d-electron spins of V(2) in the dimer remain in a spin-singlet ground state above and below T_{t}. Furthermore, $C(T_{\text{t}} < T)$ is different for A^+ and A^{2+} members. This may indicate that the observed values of $C(T_{\text{t}} < T)$ can be explained by $C_1 + C_3$ because only C_3 values are dependent on the valence of A. Therefore, we can assume V(2) as the nonmagnetic ions at all temperatures. Given the assumption on V(2), we can explain successfully the transition at T_{t} as mentioned below.

Now we discuss the transition at T_{t}. We define ΔC as the difference between $C(T_{\text{C}} < T < T_{\text{t}})$ and $C(T_{\text{t}} < T)$. From the values in table 6, we determine $\Delta C = 2.6$, 2.6 and 2.7 emu/mol K, for the Na-, Sr-, and Pb-compounds, respectively. These values of ΔC are almost the same, although the average vanadium valence is different between the A^+ and A^{2+} members. According to equation (2), the Curie constant C is proportionate to the number of paramagnetic ions and the square of their effective moments. The observed reduction of the Curie constant through T_{t} can be attributed to vanishing of a part of the paramagnetic spins at T_{t}. The important point is that the observed value of ΔC closely agrees with the calculated value of $C_1 = 3.00$ emu/mol K. In other words, the transition at T_{t} can be ascribed to disappearance of the magnetic moments of the V(1) sites. In fact, the observed values of $C(T_{\text{C}} < T < T_{\text{t}})$ closely agree with the calculated values of C_3. This means that only the V(3) ions have the paramagnetic moment below T_{t}. As discussed below, the disappearance of the V(1) moments at T_{t} is consistent with the atomic displacement caused by structural transition from the HTH- to the LTH-structure.

To compare with AV_6O_{11}, let us consider a vanadium oxide of $LiVO_2$. $LiVO_2$ has an ordered rock-salt-type structure in which the two different cations are segregated on alternate (111) cubic plane [11]. The vanadium octahedra share edges with each other and form a two-dimensional triangular lattice. It has been known that $LiVO_2$ shows a phase transition at T_{t} of about 450 K [12, 13]. The appearance of weak superlattice reflection peaks below T_{t} was reported, which indicates the formation of triangular clusters of the vanadium atoms within the basal plane [14–16]. This transition accompanies an abrupt decrease in magnetic susceptibility

[13]. The NMR study [17] indicates that the vanadium ions are in a nonmagnetic spin-singlet state below T_t. Two interpretations have been proposed for the transition so far [18, 19]. One explanation [18] is that the nonmagnetic behaviour below T_t is attributed to molecular orbital formation of the vanadium atoms, which results in quenching of the local spin moments. The other [19] is the orbital ordering mechanism, which leads to a spin-singlet ground state of the system, while the local spin configuration of each vanadium ion remains essentially unchanged. In any case, it is obvious that the atomic displacement causing the trimerization of the vanadium atoms plays an important role in the formation of the nonmagnetic ground state.

Since the structural and magnetic phase transitions occur simultaneously at $T_{t,mag} = T_t$, a strong coupling interaction between the structure and the magnetism of AV_6O_{11} is expected. As mentioned above, the V(1) atoms in AV_6O_{11} are displaced from the regular position of the kagome lattice and form triangular clusters below T_t. The trimerization of V(1) in AV_6O_{11} is quite similar to the trimerization of the vanadium atoms in $LiVO_2$; whereas the former are based on the kagome lattice, the latter are based on the triangular lattice. As is the case in $LiVO_2$, it is most probable that the trimerization of V(1) sites in AV_6O_{11} results in nonmagnetic spin-singlet formation of the V(1) spins of $S = 1$ below T_t. From the quantitative analyses of χ, we show the abrupt decrease of the Curie constants at T_t and suggest the disappearance of paramagnetic moments at V(1) below T_t. Therefore, we propose that the d-electrons at V(1) show the transition from the paramagnetic state above T_t to the nonmagnetic ground states below T_t, as is the case with the d-electrons in $LiVO_2$. This gives a most reasonable explanation for the structural and magnetic transition at T_t. Microscopic measurements such as NMR studies will be useful for confirming the spin-singlet ground state of V(1). Our ^{23}Na-NMR study carried out for NaV_6O_{11} indicates the appearance of the spin gap below T_t [20].

The change of the sign of Θ_p at T_t can be understood in this context. If each of V(1) and V(3) has paramagnetic moments for $T > T_t$, we can expect three kinds of interaction between the paramagnetic moments; V(1)–V(1), V(1)–V(3) and V(3)–V(3). The negative Weiss temperature above T_t indicates that the dominant interaction between the paramagnetic moments is antiferromagnetic. It is noted that coexistence of the ferro- and antiferromagnetic interactions cannot be ruled out because the Weiss temperature represents only the average of the interaction in the mean field theory. When the paramagnetic moments at V(1) disappear at T_t, the former two kinds of interaction will be lost in the Curie–Weiss susceptibility and therefore an abrupt change of the Weiss temperature will be achieved. The positive Weiss temperature below T_t indicates that the interaction V(3)–V(3) is ferromagnetic because the paramagnetic moments which dominate the Curie–Weiss behaviour remain only at V(3) for $T_C < T < T_t$. AV_6O_{11} shows the magnetic transition at T_C (=65 K (A = Na), 75 K (A = Sr), and 85 K (A = Pb)) and spontaneous magnetization appears below T_C. It should be noted that the value of Θ_p below T_t agrees well with the value of T_C for all the compounds. This implies that the magnetic moments at V(3), which interact with each other ferromagnetically, result in the long-range order at T_C. Nevertheless, one may find that the interaction V(3)–V(3) is rather strong in spite of the long atomic distance between V(3)–V(3) (∼5.8 Å). The origin of the strong interaction is not clear.

The increase of χ_0 at T_t may be comprehensible as an increase of the Van Vleck orbital susceptibility from V(1) which is accompanied by the spin-singlet formation. As mentioned above, $LiVO_2$ exhibits the transition at T_t of about 450 K. In spite of the nonmagnetic ground state below T_t, there remains the slight but finite temperature-independent susceptibility in $LiVO_2$, $\chi_0 \sim 1.0 \times 10^{-4}$ emu/mol, whereas the susceptibility at $T > T_t$ obeys the Curie–Weiss law and χ_0 is nearly zero [17]. The enhancement of χ_0 below T_t in $LiVO_2$ is mainly

attributed to the Van Vleck orbital susceptibility of the vanadium d-electrons [17], which is indicative of the change in the orbital state going through the phase transition of the trimerization, giving rise to the spin-singlet formation. In this paper, we have shown the similarities between the transition in $LiVO_2$ and the transition at T_t in AV_6O_{11}. If the magnetic moments at V(1) in AV_6O_{11} vanish below T_t, as is the case in $LiVO_2$, there should also remain the temperature-independent but finite susceptibility due to Van Vleck orbital susceptibility from V(1). This contribution to total susceptibility in AV_6O_{11} will cause the enhancement of χ_0 below T_t. Although the value of χ_0 in AV_6O_{11} is one order larger than that of $LiVO_2$, the quantitative discrepancy of χ_0 may originate from the fact that the vanadium atoms in $LiVO_2$ form a triangular lattice and the V(1) site in AV_6O_{11} forms a kagome lattice.

Our XRD measurements have confirmed that NaV_6O_{11} shows structural transition at 80 K from the LTH- to the O-structure. However, in contrast to the case in the Na-compound, we cannot find any evidence that either of SrV_6O_{11} and PbV_6O_{11} indicate a structural transition besides those from the HTH- to the LTH-structure at T_t. That is, the A^+ member exhibits the O-structure below 80 K, which is slightly higher than $T_C = 65$ K, while the A^{2+} members maintain the LTH-structure even at the lowest temperature. One can also find that the A^+ and A^{2+} members are also different in respect of the temperature dependence of the magnetization below T_C. It is probable that the structures and the magnetic properties around T_C are strongly related to each other. More detailed structural and magnetic studies below T_C will be needed for further discussion.

5. Conclusion

We conducted x-ray diffraction experiments over a wide temperature range for mixed valence vanadium compounds of AV_6O_{11} (A = Na, Sr, Pb) and measured their magnetic susceptibilities. We found that not only NaV_6O_{11} but also SrV_6O_{11} and PbV_6O_{11} indicate a structural transition from the HTH- to the LTH-structure at $T_t = T_{t,mag} = 245$ K (A = Na), 320 K (A = Sr) and 560 K (A = Pb). Using the Curie–Weiss law including temperature-independent susceptibility, we analysed the paramagnetic susceptibility in low ($T_C < T < T_t$) and high temperature ($T > T_t$) regions. The transition at T_t induces an abrupt decrease of the Curie constants, which indicates vanishing of the paramagnetic moments at V(1) sites. We suggest that the d-electrons of V(1), which make a kagome lattice in AV_6O_{11}, indicate a transition from the paramagnetic state above T_t to the nonmagnetic ground state below T_t, accompanied by the trimerization of the V(1) atoms. Our model gives a most satisfactory explanation for the transition at T_t.

Acknowledgments

We are grateful to Y Ikeda for his cooperation in the preliminary XRD measurements, and to Y Kanke and Y Hata for valuable discussion. This work was supported by the Scientific Research Grant-in-Aid from the Ministry of Education, Science, Sports and Culture.

References

[1] Roy M E, Besse J P, Chevalier R and Gasperin M 1987 *J. Solid State Chem.* **67** 185
[2] Kanke Y, Kato K, Takayama-Muromachi E and Isobe M 1992 *Acta Cryst.* C **48** 1386
[3] Kanke Y *et al* 1994 *J. Solid State Chem.* **112** 429
[4] Akiba A, Yamada H, Matsuo R, Kanke Y, Haeiwa T and Kita E 1998 *J. Solid State Chem.* **67** 1303
[5] Uchida Y, Kanke Y, Takayama-Muromachi E and Kato K 1991 *J. Phys. Soc. Japan* **60** 2530

[6] Kanke Y, Takayama-Muromachi E, Kato K and Matsui Y 1990 *J. Solid State Chem.* **89** 130
[7] Kanke Y, Izumi F, Takayama-Murimachi E, Kato K, Kamiyama T and Asano H 1991 *J. Solid State Chem.* **92** 261
[8] Uchida Y, Kanke Y and Onoda Y 1992 *Ferrrites, Proc. 6th Int. Conf. on Ferrites* (Tokyo: Japan Society of Powder and Powder Metallurgy) p 722
[9] Mentre O and Abraham F 1996 *J. Solid State Chem.* **125** 91
[10] Izumi F and Ikeda T 2000 *Mater. Sci. Forum* **321–324** 198
[11] Rudorff W and Becker H 1954 *Z. Naturforsch.* B **9** 613
[12] Reuter B, Weber R and Jaskowski J 1962 *Z. Electrochem.* **66** 832
[13] Kobayashi K, Kosuge K and Kachi K 1969 *Mater. Res. Bull.* **4** 95
[14] Hewston T A and Chemberland B L 1985 *J. Solid State Chem.* **59** 168
[15] Takei H, Koike M, Imai K, Sawa H, Kadowaki H and Iye Y 1992 *Mater. Res. Bull.* **27** 555
[16] Imai K, Koike M, Sawa H and Takei H 1993 *J. Solid State Chem.* **102** 277
[17] Kikuchi J *et al* 1991 *J. Phys. Soc. Japan* **60** 3620
[18] Goodenough J B, Dutta G and Manthiram A 1991 *Phys. Rev.* B **43** 10170
[19] Pen H F, Brink J, Khomskii D I and Sawatzky G A 1997 *Phys. Rev. Lett.* **78** 1323
[20] Kato H, Kato M, Yoshimura K and Kosuge K 2001 *J. Phys. Soc. Japan* at press